PKN2 regulates cell-junctions to limit colitis and colon tumour formation

Authors

Jack C Henry[1], Ashley Campbell[1], Prerana Huddar[1], Joanne Sewell[1], Shinelle Menezes[1], Adam Passman[2], Kane Smith[4], Shannah McGauran[1], Ivan Quétier[1], Meng-Lay Lin[2], Marnix Jansen[5], Neil McDonald[3], Trevor A Graham[4], Stuart McDonald[2] and Angus JM Cameron[1*].

1. Kinase Biology Laboratory, Barts Cancer Institute, Queen Mary, University of London, John Vane Science Centre, Charterhouse Square, London, EC1M 6BQ, UK
2. Barts Cancer Institute, Queen Mary, University of London, John Vane Science Centre, Charterhouse Square, London EC1M 6BQ, UK
3. Francis Crick Institute, 1 Midland Road, London NW1 1AT, UK
4. Centre for Evolution and Cancer, Institute of Cancer Research, London, SM2 5NG, UK
5. University College London Cancer Institute, Huntley Street, London, WC1E 6AG, UK

*Corresponding Author: Angus JM Cameron. e-mail: a.cameron@qmul.ac.uk

Abbreviations

AOM: Azoxymethane, ATCC: American Type Culture Collection, BSA: Bovine serum albumin, CCs3: Colon cancer susceptibility locus on mouse chromosome 3, Cdcs1: Cytokine deficiency-induced colitis susceptibility-1, COAD: Colon adenocarcinoma (TCGA), CreERT2: Tamoxifen-inducible Cre recombinase, DAPI: 4′,6-diamidino-2-phenylindole, DAI: Disease Activity Index, DMEM: Dulbecco's Modified Eagle Medium, DMSO: Dimethyl sulfoxide, DSS: Dextran sodium sulphate, EDTA: Ethylenediaminetetraacetic acid, EGTA: Ethylene glycol-bis(β-aminoethyl ether)-N,N,N′,N′-tetraacetic acid, FBS: Fetal bovine serum, FFPE: Formalin-fixed paraffin-embedded, FITC: Fluorescein isothiocyanate, GEO: Gene Expression Omnibus, GSVA: Gene Set Variation Analysis, GSEA: Gene Set Enrichment Analysis, H&E: Haematoxylin and eosin, HET: Heterozygous, HRP: Horseradish peroxidase, IBD: Inflammatory bowel disease, IBS : Irritable bowel syndrome, IL-1β: Interleukin-1 beta, IL-6: Interleukin-6, iPKN2^{KO}: Inducible PKN2 knockout, JAM-A: Junctional adhesion molecule A, KD: Kinase-dead, KEGG: Kyoto Encyclopedia of Genes and Genomes, KO: Knockout, LPS: Lipopolysaccharide, PBS: Phosphate-buffered saline, PCA: Principal Component Analysis, PFA: Paraformaldehyde, PKN2: Protein kinase N2, PVDF: Polyvinylidene fluoride, READ: Rectal adenocarcinoma (TCGA), SDS–PAGE: Sodium dodecyl sulphate–polyacrylamide gel electrophoresis siRNA: Small interfering RNA, TAM: Tamoxifen / 4-hydroxytamoxifen, TCGA: The Cancer Genome Atlas, TBS: Tris-buffered saline, TNF-α: Tumour necrosis factor alpha, UMI: Unique molecular identifier, Vil1-CreERT2: Villin promoter-driven inducible Cre line, WT: Wild-type, ZO-1: Zona occludens-1

Abstract

Background and Aims

Epithelial barrier integrity in the gut must be tightly regulated to allow essential paracellular transport while limiting mucosal exposure to inflammatory microbes and toxins. Chronic inflammation in inflammatory bowel diseases is a major health burden and a key risk factor for colorectal cancer. Here, we identify the Rho-regulated kinase PKN2 as a non-redundant safeguard of epithelial barrier integrity and a candidate tumour suppressor in colorectal cancer.

Methods

Conditional PKN2 knockout mouse models were used to examine the impact of PKN2 loss on colitis severity and induction of colorectal adenomas. Intestinal organoid models, epithelial barrier assays and bioinformatic approaches explored PKN2 regulation of epithelial function. Human inflammatory bowel disease datasets are analysed for associations with PKN2 expression and signatures associated with compromised barrier integrity.

Results

PKN2 deletion sensitises mice to inflammatory bowel injury and promotes colorectal adenoma formation in a colitis-associated colorectal cancer model. Tumour burden tightly correlates with colitis severity suggesting that enhanced inflammation-driven tissue injury underlies tumour promotion. Mechanistically, PKN2 localises to epithelial tight junctions and is required to stabilise barrier integrity during epithelial injury in mouse and organoid models. Transcriptomic changes associated with epithelial PKN2 loss mimic inflammatory bowel diseases and correlate with diseases severity and therapy response in human datasets.

Conclusions

PKN2 is a regulator of gut barrier integrity encoded at genomic loci previously associated with sensitivity to bowel inflammation and tumour suppression in both humans and mice. PKN2 loss recapitulates key features of human colitis and implicates PKN2 as a regulator tight junction integrity that shapes disease severity, treatment response and cancer risk.

Keywords

PKN2; inflammatory bowel disease; intestinal permeability; colitis-associated colorectal cancer.

Introduction

Inflammatory bowel disease (IBD), comprising Crohn's disease and ulcerative colitis, is a group of chronic inflammatory disorders of the gastrointestinal tract, with a prevalence of approximately 0.3% in Western populations and a rising incidence in newly industrialized countries[1]. It is well established that patients with IBD have a significantly higher risk of developing colorectal cancer compared to the general population and therefore often undergo regular colorectal screening tests to detect and remove pre-malignant lesions[2-4]. Chronic inflammation plays a central role in the development and progression of many cancers, including both sporadic and colitis-associated colorectal cancer. Supporting this, anti-inflammatory drugs such as Aspirin and COX inhibitors have been shown to significantly reduce the risk of developing sporadic colorectal cancer[5-8]. In experimental models, disrupting inflammatory pathways, both intrinsic to epithelial cells and through immune cell targeting, reduces tumour formation in both the azoxymethane/dextran sodium sulphate (AOM/DSS) and genetic APC-targeting models[9-12].

Given the strong link between inflammation and colorectal cancer risk, there has been considerable interest in identifying genetic loci that predispose individuals to IBD. Chromosome arm 1p has been identified as a significant susceptibility locus for human IBD; however, it contains over a thousand genes, making it difficult to pinpoint candidates[13]. Two potential candidates on 1p36 include TNF receptor and Caspase 9, yet other candidates on 1p are yet to be discovered[14, 15]. Genetic mouse studies have implicated regions on chromosome 1p by exploring differential sensitivity in different background strains. *Cdcs1 (cytokine deficiency-induced colitis susceptibility-1)* on chromosome 3 is a locus containing 340 genes, syntenic with human 1p. Cdcs1 is well characterised as the cause of increased susceptibility between different mouse strains in several knockout colitis models[16]. Further research also identified the overlapping (colitis-associated) colon cancer susceptibility locus on mouse chromosome 3 (CCs3), which drives increased susceptibility to AOM/DSS-induced colorectal tumours in the A/J mouse strain when compared to C57BL/6J[17].

Here, we identify PKN2 as a key colitis susceptibility gene on human chromosome 1p, syntenic with murine *Cdcs1* and CCs3. Global or epithelial-specific loss of PKN2 in vivo sensitises mice to DSS-induced colonic injury and promotes colorectal adenoma formation. Mechanistically, PKN2 deficiency disrupts epithelial tight junction integrity and barrier permeability, providing new insight into the pathogenesis of colitis and colorectal cancer.

Methods

Mouse models

All animal procedures were approved by the Queen Mary University of London ethics committee and performed under the UK Home Office Animal and Scientific Procedures Act (1986). Both sexes were included, with no sex-dependent differences observed.

PKN2 knockout

Conditional Pkn2$^{fl/fl}$ mice were crossed with B6.129-Gt(ROSA)26Sortm1(cre/ERT2)Tyj/J (JAX:008463) or B6.Cg-Tg(Vil1-cre/ERT2)23Syr/J (JAX:020282) mice. Pkn2$^{fl/fl}$ mice were generated as previously described[18]. PKN2 deletion was induced using five daily intraperitoneal injections of tamoxifen (100 mg/kg in corn oil), followed by a 20-day recovery period.

AOM/1%DSS model

Following PKN2 knockout, mice received 1x intraperitoneal injection of azoxymethane (10mg/kg in PBS, 0.45µm-filtered, Sigma Aldrich), followed 3 days later by 3x cycles of dextran sodium sulphate (1/2% DSS in drinking water; 5 days, refreshed day 2, 16day recovery; Figure 1A; MP Biomedicals). Tumours were analysed 40 days after the final DSS cycle.

Disease activity was assessed using a composite score of weight loss, stool consistency, haematochezia and general condition (1-3 per parameter, max 12) [19]. Mice were sacrificed immediately upon a score of 3 in either weight loss or general condition, or after 24h of unresolved score 3 for stool consistency or haematochezia. Scoring was performed semi-blind.

DSS only models

Mice received 5 days of DSS (1/2% in drinking water, refreshed day 2) and were sacrificed 3/10 days later.

Histology and immunohistochemistry

Colons were excised, Swiss-rolled[20], fixed, paraffin-embedded and sectioned. Slides were dewaxed, rehydrated, subject to antigen retrieval (sodium citrate pH 6.0 10mM) and blocked with 3% hydrogen peroxide (Thermo-Fisher). Slides were then stained with CD4 (Thermo-Fisher, 14-9766-82), CD8 (Thermo-Fisher, 14-0808-82), F480 (Abcam, MCA497R), Ki67 (GeneTex, GTX16667), CD45 (Biolegend, 103101) and ZO-1 (Thermo-Fisher, 617300) overnight at 4°C and detected using Universal Vectastain ABC kit with Dab substrate (Dako, K3468). Slides were counterstained using haematoxylin (Sigma Aldrich) and mounted in DPX (Sigma Aldrich). Alcian Blue staining used 8GX 1% in 3% Acetic Acid (RRSK400-100).

Slides were scanned using a Nanozoomer-S210 (Hamamatsu) and analysed using QuPath (v0.5.1) [21]. Erosion and submucosa length were averaged per mouse across multiple sections. Immune infiltrates were quantified through positive cell detection, alcian blue staining by random forest–based area quantification, and ZO-1 depletion by DAB intensity thresholding within an 18µm luminal region.

Tissue culture

Cell lines

DLD1 (ATCC), HEK293T (ATCC), Caco-2 and L-WRN cells were maintained in DMEM plus 10% FBS and 100U/ml penicillin/streptomycin (Gibco) under standard conditions (37°C, 5% CO_2). Cell lines were routinely passaged using trypsin–EDTA (Gibco) and cryopreserved in 10%FBS/DMSO. Caco-2 were gifted from Egle Solito and L-WRN cells[22] from Chris Tape.

Organoid production and culture

Crypts of 12-week-old wild-type C57BL/6 and *Pkn2*$^{fl/fl}$*;Rosa26-CreER*^{T2} mice were isolated by 2mM EDTA dissociation and embedded in growth-factor-reduced Matrigel (Corning) as described[23]. Organoids were cultured in Advanced DMEM/F-12 (Gibco), plus 2mM L-glutamine (Gibco), 1mM N-acetyl-l-cysteine (Sigma), 10mM HEPES (Sigma), B-27 (Gibco, 50X), N-2 (Gibco, 100X), HyClone Penicillin/Streptomycin (Cytiva), 10mM nicotinamide (Merck), 50ng mL−1 mEGF (PeproTech) and 25% WRN-conditioned media at standard conditions (37°C, 5% CO_2). PKN2 knockout was induced by 4-hydroxytamoxifen (2µM TAM, 7-day treatment; Merck) and passaged every 7–10 days by mechanical dissociation. WRN-conditioned medium was generated from L-WRN cells as previously described[22].

Generation of PKN2 knockout/knockdown cell lines

CRISPR-Cas9 PKN2 knockout

Human PKN2 targeting (CTTTGACGTGGACTTAGTGT-Exon 6) and non-targeting (GTATTACTGATATTGGTGGG) gRNA were cloned into the Lenti-Cas9-gRNA-GFP plasmid (Addgene #124770; gifted by Jason Sheltzer) as described[24]. Lentiviral particles were generated in HEK293T cells using a calcium phosphate–based transfection approach (ProFection). Viral supernatants were collected and clarified before addition to DLD1 cells for 24h (50% media mix with 8µg/mL polybrene). GFP-positive cells were isolated by flow cytometry (ARIA Fusion).

Inducible PKN2 expression

Stable inducible DLD1 (iDLD1) cells were produced by the integration of wild-type or kinase-dead PKN2 constructs (pcDNA5/FRT/TO/PKN2(WT/D782A)) in DLD1-FRT cells containing the Flp-In™ T-REx™ system (Invitrogen) (gifted by Stephen Taylor). After antibiotic selection (hygromycin (100µg/ml; Invitrogen)/blasticidin (10µg/ml; Thermo-Fisher)) for 30 days, transgene expression was induced with tetracycline (500ng/ml; Sigma).

siRNA knockdown

DLD1 cells were transfected with 20nM siRNA control (siCtrl #1) or PKN2 (siPKN2 #9, 10 & 11) pools (GE HealthCare) using Lipofectamine™ LTX (Thermo-Fisher) according to manufacturer's instructions.

Immunofluorescence

Cells or organoids were seeded onto coverslips, Nunc Lab-Tek II 8 well Chamber Slides (Thermo-Fisher) or 96-well PhenoPlates (Revvity). Cells or organoids were fixed with 4% PFA (organoids 2h, cells 15min; Thermo-Fisher), permeabilised with 0.2% Triton X-100 (15min; Sigma), blocked with 5% BSA (1h; Sigma), and incubated with PKN2 (R&D, MAB5686), ZO-1 (Invitrogen, 61-7300) or E-cadherin (Cell Signaling Technology, 3195T) overnight at 4 °C. PKN2 signal was amplified using Alexa Fluor™ 488 or 555 Tyramide SuperBoost (Invitrogen) according to the manufacturer's instructions. Samples were incubated with DAPI, Phalloidin (Invitrogen, A22283), anti-Rabbit IgG Alexa Fluor™ 488/555/633 (Invitrogen, A-21206, A-31572, A-21071) or anti-Mouse IgG Alexa Fluor™ 488/555 (Invitrogen, A-11001, A-31570) and mounted in MOWIOL or left in PBS, and imaged by LSM 880 confocal microscope (Zeiss) or high-content IN Cell Analyzer 6000 (Cytiva). Image analysis was performed using Fiji ImageJ (v2) or CellProfiler (v4.2.8).

Junctional staining analysis

A CellProfiler (v4.2.8) pipeline was assembled to perform junctional analysis. ZO1-stained junctions were enhanced using morph "openlines" (length 30) and "neurite-like" features enhanced with "tubeness" (smoothing 2). Enhanced junctions were smoothened (circular average filter & diameter of 4) and converted into junction objects using global robust background thresholding. Objects were filtered by minimum major axis length of 5.4µm to remove punctate artefacts and measurements taken. ZO1 junctional intensity was measured by masking the original image with the junction objects.

Epithelial barrier permeability assays

DLD1 cells were seeded onto 0.4µm Pore Transwells (Corning) and cultured for 7 days under standard conditions. Monolayers were treated with control medium, 2h 50mg/ml DSS or 30mins 4mM EGTA, washed, and permeability assessed using 40kda FITC Dextran (5mg/ml in Phenol red-free DMEM, Merck). Flow-through samples were collected after 3h and measured at 485/535nm on FLUOstar OPTIMA microplate reader (BMG LABTECH).

Organoids embedded in Phenol Red-Free Matrigel (Corning) on a 96-well PhenoPlate (Revvity) were treated with either 2h 4mM EGTA, 96h inflammatory cocktail ((100ng/ul LPS (Sigma), 30ng/ml of IL-1β, IL-6, TNF-α (Gibco)), 48h 10µg/ml DSS or a combination thereof. Permeability was assessed with 4kda FITC Dextran (Merck). After 2h, images were taken by LSM 880 confocal microscope (Zeiss) and internalised dextran (%) was calculated using Fiji (v2).

Molecular biology

Western blotting

Powdered snap frozen tissue or cultured cells were lysed in NuPAGE LDS (Invitrogen) with 50mM DTT (Sigma-Aldrich), sonicated, and boiled at 95°C for 5mins. Protein concentration measured by DC protein assay kit (Bio-Rad), separated by SDS–PAGE (4–12% Bis-Tris gels (NuPAGE)) and transferred to nitrocellulose (Amersham) or PVDF (Millipore) membranes overnight (4°C). Membranes were blocked in 3% BSA TBS–Tween (0.1%) (Sigma) and incubated overnight (4°C) with primary antibodies, PKN2 (R&D MAB5686), GAPDH (Santa-Cruz SC-25778) or HSC70 (Santa-Cruz SC-7298), followed by HRP-conjugated secondary antibodies (GE Healthcare NXA931) and chemiluminescent detection (Luminata Forte/ Crescendo (Merck)).

PCR genotyping

DNA was extracted from EGTA-dissociated colon crypts (tamoxifen treated *Pkn2*$^{fl/fl}$*;Vilin-CreER*^{T2}), organoids (QIAamp mini-DNA kit (Qiagen)) and FFPE sections (GeneJET FFPE DNA Purification Kit (Thermo-Fisher)). Multiplex PCR was performed (DNA using Platinum™ II Hot-Start PCR Master Mix (Thermo-Fisher)) using primers spanning the PKN2 alleles (GCATGCTGAGGATGTCACCG, GAGGGAAAATGGGAGAGG and GCAGTGGTGAAGTCACATAC). Samples were run alongside a 50bp ladder (NEB), on a 6% TBE gel (Thermo-Fisher), incubated with GelGreen (Merck) and imaged on a ChemiDoc-MP (Bio-Rad).

RNA sequencing and bioinformatic analysis

All primary RNA sequencing data are deposited onto the Gene Expression Omnibus (GEO) under project accessions GSE313373 (adenomas) and GSE313375 (organoids). All analysis was performed using custom R (V4.4) or bash scripts available on GitHub (https://github.com/jackchenry/PKN2_in_CA-CRC). Visualisations were produced with ggplot2 (v3.5.1), ComplexHeatmap (v2.20) and GraphPad Prism (v10.1.6). Differential expression analysis was performed using DeSeq2 (v1.44) and gene-set enrichment analysis using fgsea (v1.30) with gene-sets from the molecular signatures database (v2024.1.Hs; v2024.1.Mm).

RNA sequencing

RNA was extracted using the Qiagen RNAeasy mini kit (QIAGEN) and quality assessed using a 5300 Fragment Analyzer (Agilent Technologies). Poly(A) selection Library preparation and paired-end RNA sequencing was performed by GENEWIZ (Azenta) using NovaSeq™ 6000 (Illumina). Trimming, aligning to GRCm39 and counting was performed using trimmomatic (v0.36), STAR (v2.7.9), samtools (v1.19.2) and subread (v2.0.6) using annotation files from GENCODE (M34).

Smart-3SEQ sequencing

Laser capture microdissection was used to isolate epithelial regions from FFPE sections, followed by Smart-3SEQ library preparation as previously described[25, 26]. RNA quality was assessed using a Tapestation Fragment Analyser (Agilent Technologies) and sequenced using the Illumina NextSeq 2000 at the Genome Facility (ICR). FASTQ were processed as above with the addition of deduplication using umi_tools (v2.0.6).

External data and integrative analysis

Public RNA datasets were obtained from the Genomic Data Commons data portal (https://portal.gdc.cancer.gov/) and Gene Expression Omnibus under accessions GSE102746[27], GSE193677[28], GSE206285[29], GSE109142[30], GSE117993[30], GSE207022[31], GSE16879[32], GSE59071[33], GSE95437[34], GSE235236[35], GSE243625[36], GSE53306[37], GSE52746[38]. Known cancer genes were obtained from COSMIC. The PKN2^{KO} signature was created using organoid differential expression and GSVA. Immune infiltrate deconvolution was performed as previously described[39]. Single-cell RNA data was obtained from PREDICT[40]. PKN2 proteomic data was obtained from the source publication[41]. PrismEXP prediction results on ARCHS4 data was obtained for PKN2 from the ARCHS4 data portal (v2.5, https://archs4.org/)[42]

Results

PKN2 loss promotes colitis and colitis -associated colorectal cancer

To test if PKN2 can act as a colitis-associated tumour suppressor, we exploited our inducible conditional PKN2 knockout mouse (global-iPKN2^{KO}: *Pkn2$^{fl/fl}$;Rosa26-CreER^{T2}*) and the two-stage azoxymethane (AOM)/Dextran sodium-sulphate (DSS) colitis-associated colorectal tumour model (Figure 1A). Global PKN2^{KO} is embryonic lethal[18], but inducible conditional deletion in adults is generally well-tolerated[18, 43] with minimal macroscopic effects on normal colon homeostasis. Five consecutive days of treatment with tamoxifen in the iPKN2 model was sufficient to activate Cre and induce loss of PKN2 DNA and protein in the intestines of adult mice (Figure S1A, B)[21]. To induce tumours, WT and PKN2 targeted mice were treated with a single dose of the mutagen AOM (10mg/kg) followed by three repeated rounds of 1% DSS, which typically results in tumour formation at 90 days[44]. Typically, DSS is administered at 2-2.5% in C57BL/6 mice but pilot experiments indicated that PKN2 targeted mice tolerated 2% DSS regimens poorly (Figure S1C-E). Even at the reduced dose of 1% DSS, both heterozygous (global-iPKN2^{HET}) and homozygous PKN2 (global-iPKN2^{KO}) deletion significantly exacerbated weight loss, disease activity and survival (scored 1-14) [19] (Figure 1B-G). Surviving mice with PKN2 loss continued to show increased weight loss and disease activity across the experimental time course (Figure S1F-I). At 90-days post-AOM, mice were examined for tumour induction, which revealed an increase in macroscopically visible tumour incidence, multiplicity and tumour burden in PKN2-targeted mice (Figure 1H-K). No tumours were observed at 90 days in cohorts treated with AOM alone. Pathological analysis identified that global-iPKN2^{KO} bowels presented with more high-grade tubular adenomas, while incidence of low-grade tissue dysplasia and tumour size distribution was similar between genotypes (Figure S1J-L). Globally targeting PKN2 did not induce polydipsia or alter relative DSS dose (Figure S1M). PKN2 targeted mice also presented with splenomegaly (Figure S1N, O) but had no change in colon length or overt pathology associated with other organs (Figure S1P). We conclude that haploinsufficiency of PKN2 is sufficient to exacerbate DSS induced disease and colorectal cancer adenoma formation, and that homozygous loss induces a more penetrant phenotype.

We sought to characterise the adenomas to identify phenotypes associated with PKN2 loss. Immunohistochemical analysis of immune cell markers and ki67 expression identified no obvious differences in immune cell infiltrate or proliferation between genotypes (Figure S2A-E). To further explore the adenoma phenotypes, we performed Smart-3SEQ transcriptomics[25] on a selection of laser-captured epithelial regions for each genotype. Importantly, PKN2 expression is significantly reduced in heterozygous and homozygous knockouts of PKN2 (Figure S2F). However, principal component analysis identifies largely overlapping clustering between genotypes (Figure 1L),

reflecting a random, varied tumour population in which PKN2 status does not consistently dictate selected tumour phenotypes. In addition, gene set enrichment analysis between wild-type and global-iPKN2^{KO} adenomas does not identify any clear increase in cancer hallmarks or oncogenic signalling pathway activity, including APC/WNT, RAS, TP53 and YAP (Figure S2G, H). One of the most significant negatively enriched gene sets are genes upregulated by a constitutively active (Q63L) form of RHOA, a regulator of PKN2. Interestingly, six pathways were also significantly enriched in KO adenomas from the mouse tumour phenotypes ontology collection of gene sets, including tumour incidence by chemical induction, tumour growth size and metastatic potential, suggesting PKN2 might antagonise the expression of pro-tumorigenic genes in this model (Figure 1M, N, S4I).

The increased sensitivity to DSS and high-grade dysplasia incidence, coupled with largely similar adenoma transcriptomic profiles, led us to hypothesise that PKN2 loss may act primarily by exacerbating a pro-neoplastic environment. This is further supported by exquisitely tight correlation between tumour burden and average disease activity (Figure 1O).

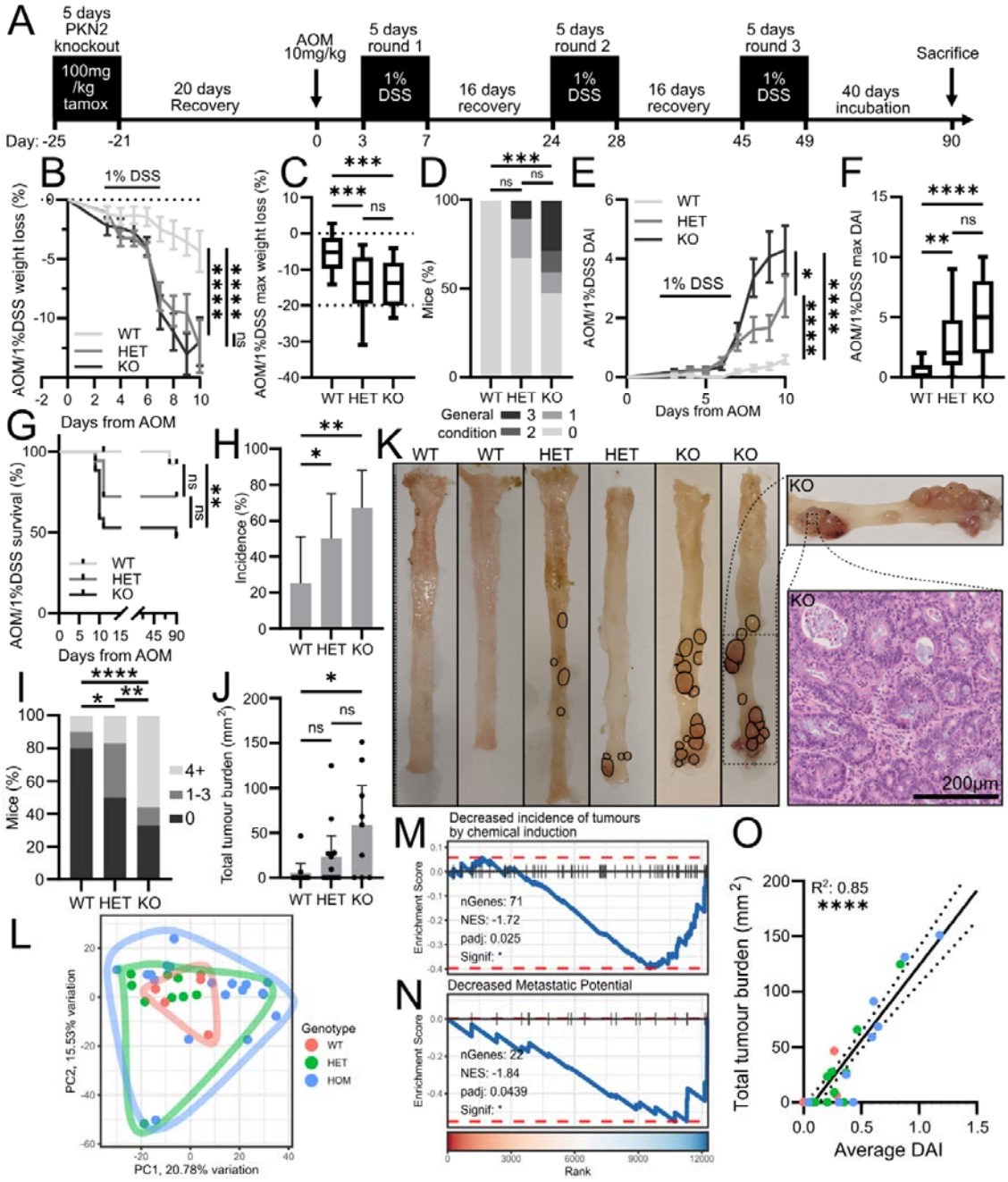

Figure 1: PKN2 loss sensitises mice to AOM/DSS treatment and promotes colitis-associated colorectal cancer. A) Schematic of the AOM/1% DSS protocol. **B, C)** Average (B) and maximum (C) weight change during the first 10 days of AOM/DSS treatment (WT: n=17, HET: n=18, KO: n=17; two-way RM-ANOVA (B), Tukey's test (C). **D)** General condition scores (0-3) during the first 10 days of treatment (WT: n=17, HET: n=18, KO: n=17; Dunnett's test). **E, F)** Average (E) and maximum (F) disease activity index (DAI) (WT: n=17, HET: n=18, KO: n=17; two-way RM-ANOVA (E), Tukey's test (F)). **G)** Kaplan Meier survival analysis (WT: n=17, HET: n=18, KO: n=17; Log-rank test). **H-J)** Adenoma incidence (H), multiplicity (J) and burden (K) at day 90 (WT: n=10, HET: n=12, KO: n=9; χ^2 test (H, I);

Dunn's test (J)). **K)** Representative colon images following the AOM1%DSS model with example pathology. **L)** PCA of Smart3-SEQ epithelial samples (WT: n=5, HET: n=10, KO: n=18 adenomas). **M, N)** Gene set enrichment analysis of KO vs WT adenomas using mouse tumour phenotypes ontology gene sets. **O)** Correlation of tumour burden and average disease activity (WT: n=10, HET: n=12, KO: n=9).

PKN2 loss aggravates inflammatory bowel injury

We next examined the impact of PKN2 loss on acute DSS treatment. Bowels harvested 8-days post initiation of 1% DSS treatment presented regions of epithelial erosion, exudate, goblet cell depletion and crypt damage with the most severe phenotypes associated with PKN2 loss (Figure 2A-E).

Single-cell RNA sequencing studies of normal and Crohn's disease inflamed human colon identify PKN2 expression is enriched in, but not restricted to, epithelial cells (Figure S3A, B). To explore if sensitisation to inflammatory bowel injury reflects an epithelial-specific role for PKN2, the PKN2^{flox} mouse was crossed onto the Villin-Cre (*Pkn2*$^{fl/fl}$*;Vil1-CreER*^{T2}) specific driver, allowing for intestinal epithelial-specific knockout of PKN2 (Epi-iPKN2^{KO}). PCR analysis of isolated epithelial crypts two weeks following tamoxifen treatment identified strong PKN2 locus recombination in the epithelial compartment of epi-iPKN2^{KO} mice (Figure S3C). Following a 2% DSS treatment regime without AOM, PKN2^{KO} mice show a similar sensitisation to the global- PKN2^{KO}, with exacerbated weight loss and DAI scores (Figure 2F, G). Bowel tissue harvested 8-days post 2% DSS treatment also presented with a significant decrease in total colon length (Figure S3D) but no change to spleen size (Figure S3E). Histologically, mice with epithelial-specific PKN2 loss also had an increased prevalence of erosions, crypt loss and depletion of goblet cells (Figure 2H, 2I, S3F, S3G). Erosions were primarily localised to distal regions in all genotypes. On average, distal submucosae showed increased thickness in global and epi-iPKN2^{KO} mice with higher levels of cellularity and CD45+ immune cell infiltrate (Figure 2J-L, S3H-L). Surrounding distal crypts also contained more CD45+ immune cell infiltrate, indicating heightened local inflammation (Figure S3M, N). These analyses indicate that either homozygous or heterozygous PKN2 loss in the epithelial compartment is sufficient to aggravate inflammatory bowel injury.

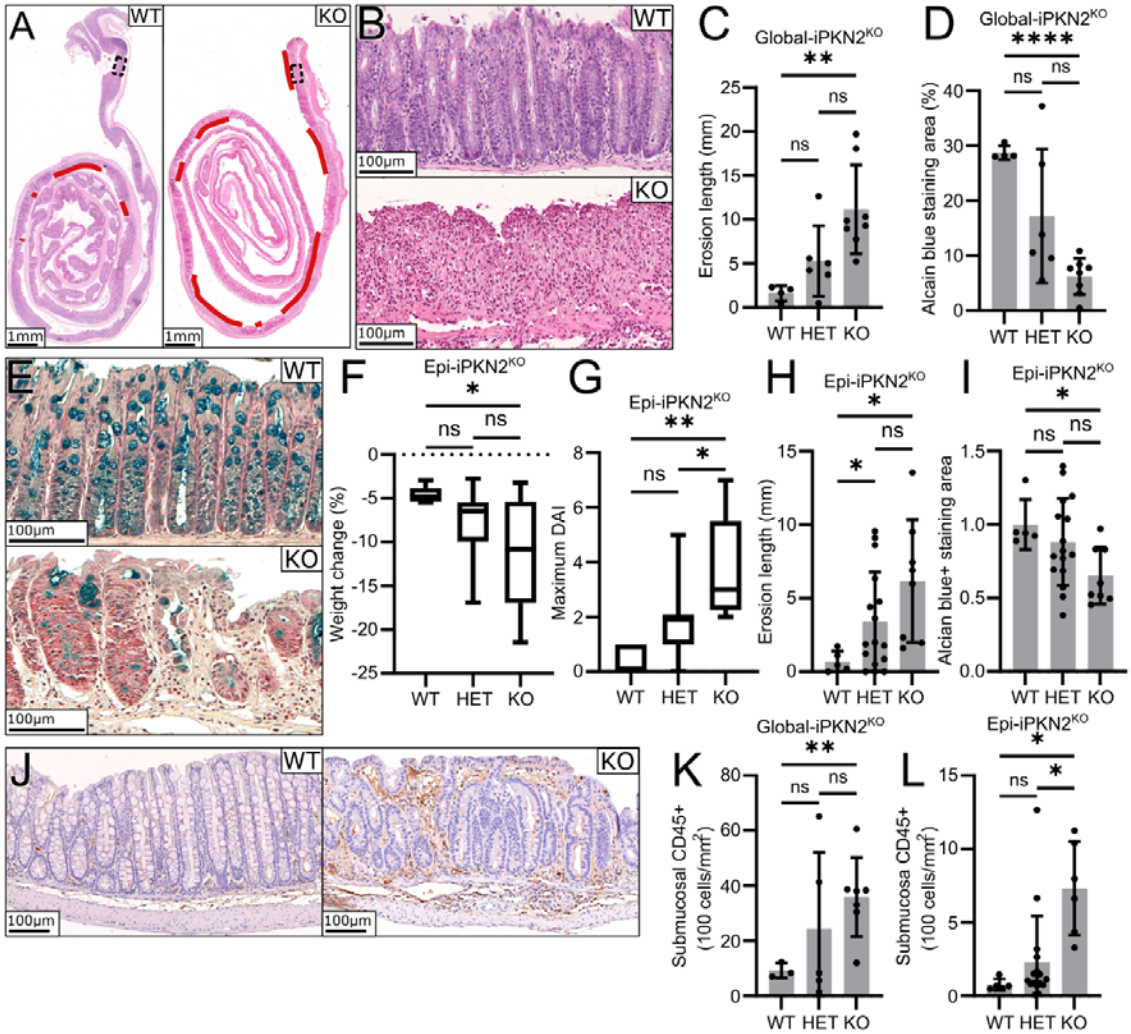

Figure 2: Epithelial PKN2 loss aggravates inflammatory bowel injury. A-C) Epithelial erosion 8 days after AOM/1%DSS treatment in global-iPKN2^{KO} mice (WT: n=4, HET: n=6, KO: n=8; Dunnett's test). Erosions are indicated in red and region shown in (B) is expanded in (A). **D, E)** Goblet cell depletion assessed by alcian blue staining following AOM/1%DSS treatment in global-iPKN2^{KO} mice (WT: n=4, HET: n=6, KO: n=8; Dunnett's test). **F, G)** Maximum weight loss and disease activity index (DAI) during the first 10 days of 2%DSS treatment in epi-iPKN2^{KO} mice (WT: n=5, HET: n=16, KO: n=8; Tukey's test). **H, I)** Erosion length (H) and goblet cell depletion following 2%DSS treatment in epi-iPKN2^{KO} mice (WT: n=5, HET: n=16, KO: n=8; Dunnett's test). **J-L)** CD45+ immune cell infiltration into distal submucosa in global-iPKN2^{KO} mice following AOM/1% DSS treatment (J, K; WT: n=3, HET: n=5 KO: n=7) and epi-iPKN2^{KO} mice in response to 2%DSS treatment (L; WT: n=5, HET: n=16, KO: n=6; Dunnett's test).

PKN2 loss perturbs ZO-1 tight junctions and models' human colitis

To investigate epithelial phenotypes in vitro, colonic organoids were generated from wild-type C57BL/6 and *Pkn2*$^{fl/fl}$*;Rosa26-CreER*^{T2} mice, enabling the inducible deletion of PKN2 with 4-hydroxytamoxifen (TAM) treatment (Figure S4A). Wild-type organoids treated with tamoxifen served as controls. RNA sequencing revealed that PKN2 loss was the dominant source of transcriptional variance, with tight clustering of biological replicates by principal component analysis (Figure S4B), PKN2 is the most significantly downregulated gene, confirming penetrant deletion (Figure S4C). While differential expression analysis identified modulation of several cancer-associated genes, PKN2-deficient organoids showed no evidence of spontaneous transformation (Figure S4D). Comparison with human IBD biopsies and colitis-derived organoids revealed substantial overlap in hallmark GSEA signatures, indicating that epithelial PKN2 loss recapitulates key transcriptional features of human colitis (Figure 3A).

Using our PKN2^{KO} epithelial transcriptional signatures, we applied PrismEXP predictions across the ARCHS4 compendium of integrated RNA-sequencing datasets to assess associations with human disease phenotypes. This revealed significant links to rectal prolapse, hematochezia and colon cancer (Figure S4E), all of which were exacerbated in our PKN2^{KO} mouse models. To relate these phenotype associations to human epithelial transcriptional changes, we derived a PKN2^{KO} epithelial signature from differentially expressed genes in PKN2-deficient organoids. Bulk PKN2 expression showed inverse correlation with this signature, consistent with reduced PKN2 expression driving a PKN2^{KO} transcriptional program (Figure S4F). Across 11 of 12 independent human IBD cohorts, the PKN2^{KO} signature was significantly elevated in both Ulcerative colitis and Crohn's disease compared with healthy controls (Figure 3B). Signature scores were higher in active versus inactive disease, enriched in inflamed compared with non-inflamed regions and maximal in distal colonic samples, mirroring observations in mouse models (Figure 3C, S4G). Notably, PKN2^{KO} scores were highest in patients with severe disease, linking loss of epithelial *PKN2* activity to disease severity and highlighting its potential importance in driving clinically aggressive inflammatory pathology in human IBD (Figure 3D).

Phenotypically, samples exhibiting an epithelial PKN2 loss-like signature showed expansion of inflammatory monocytes, fibroblasts, dendritic cells and mast cell fractions, indicating a shift toward an activated innate immune and stromal microenvironment (Figure 3E). Minimal correlation with macrophage and myofibroblast populations was observed, suggesting a stronger association with active inflammation over tissue repair (Figure 3E). Concordantly, GSEA revealed amplification of TNFα–NFκB and IL2-STAT5 driven inflammatory programs that sustain pathogenic T-cell responses and promote non-resolving mucosal injury (Figure 3G). Notably, the PKN2^{KO} score also predicted response to anti-TNF therapy, linking epithelial PKN2 loss to clinically actionable inflammatory states (Figure 3F). GSVA also demonstrated associations with inflammation, colitis and recurrent infection gene sets. Limited enrichment of gene sets involved in neoplasm-related programs further suggests that PKN2 loss promotes inflammatory damage-linked tumorigenesis rather than driving direct oncogenic programs, consistent with our in vivo findings (Figure 3G).

To gain some mechanistic insight into these transcriptional and clinical associations, we applied PrismEXP analysis on KEGG gene sets and found that PKN2 expression is strongly linked to cell junction organisation, mechanotransduction and transcriptional misregulation (Figure 3H). Consistent with this, hallmark apical junction gene sets were concordantly enriched in PKN2^{KO} organoids, IBD biopsies and samples with high PKN2^{KO} scores (Figure 3A, G). More detailed junctional analysis revealed that elevated PKN2^{KO} scores were specifically associated with gene programs

favouring junction disassembly over assembly, with a preferential loss of tight junction over adherens junction components (Figure 3G). Zona occludens-1 (ZO-1) immunostaining is commonly used to assess tight junction integrity in human intestinal tissue[45, 46]. Immunostaining of colon sections revealed a marked reduction in ZO-1–positive area in both global and epithelial-specific PKN2^{KO} mice eight days after DSS treatment (Figure 3I-K). Reduced ZO-1 staining was also evident in non-DSS treated mice two weeks following PKN2 deletion, although less pronounced at 15-days following DSS exposure (Figure S4H, I).

In line with impaired junctional stability, PKN2^{KO} organoids exhibited a strong enrichment of epithelial–mesenchymal transition programs, consistent with a shift toward wound-healing–like, junction-deficient epithelial states (Figure 3A, G). PKN2-low colon (COAD) and rectal (READ) adenocarcinoma in TCGA data similarly showed significant enrichment in apical junction gene signatures, indicating this epithelial vulnerability may be preserved in epithelial-derived bowel cancers (Figure S4J, K). Together, these analyses demonstrate that loss of PKN2 recapitulates key features of human colitis and implicates PKN2 as a central regulator of epithelial junctional integrity that shapes disease severity and colitis-associated cancer risk.

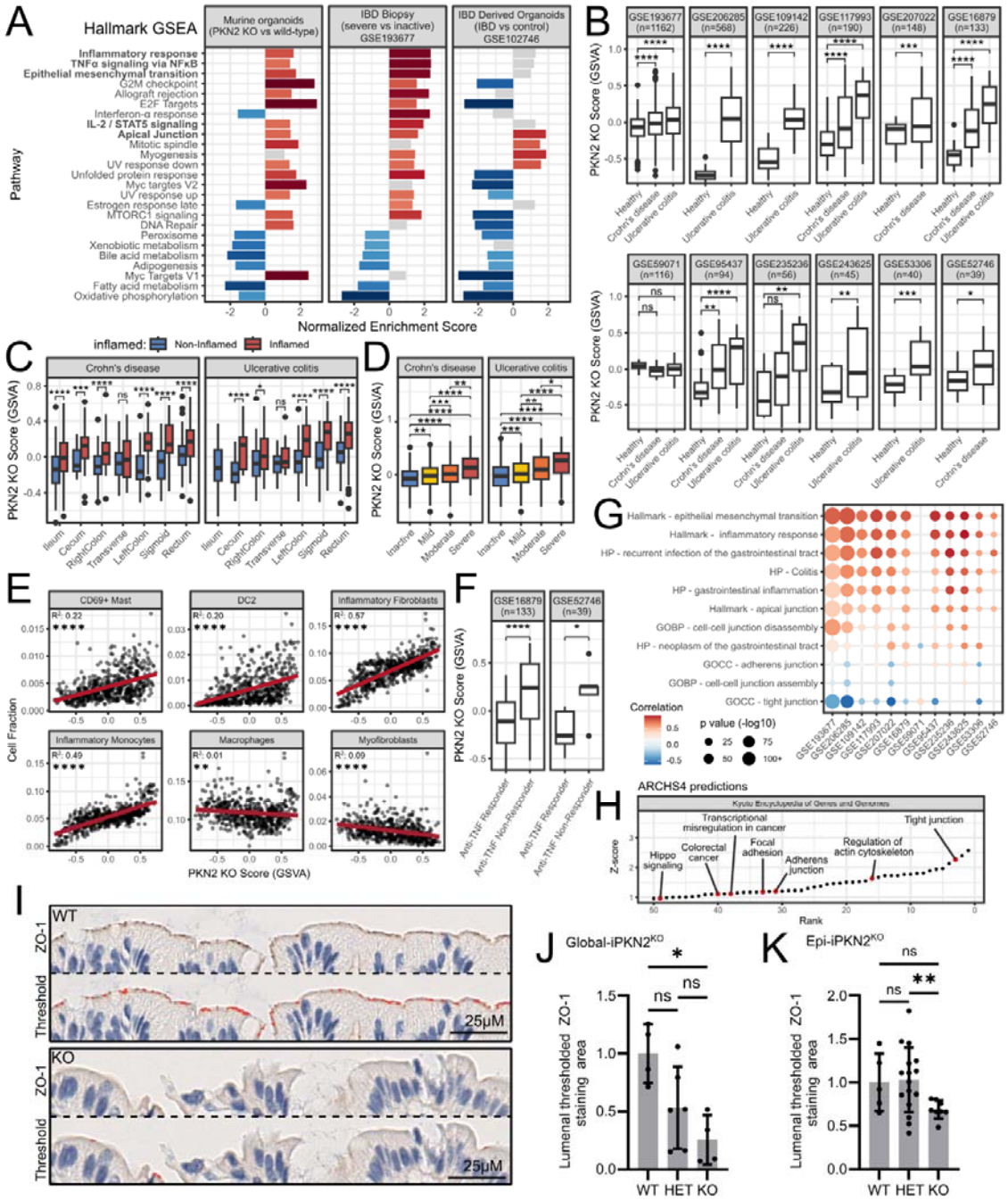

Figure 3: Transcriptomic profiling of PKN2 loss reveals inflammatory and junctional pathway modulation. A) Hallmark gene set enrichment analysis comparing transcriptional responses to $PKN2^{KO}$ in organoids with differential expression in patients with severe versus inactive IBD and primary colitis organoids versus healthy controls. **B)** $PKN2^{KO}$ score in patients with Crohn's and ulcerative colitis compared with healthy controls across 12 independent bulk RNA-sequencing and microarray datasets. **C, D)** $PKN2^{KO}$ score in inflamed versus non-inflamed bowel regions (C) and across disease severity defined by endoscopic assessment (D). **E)** Correlation between $PKN2^{KO}$ score and immune cell infiltration; line of best fit, R^2 and significance levels shown. **F)** $PKN2^{KO}$ score in Anti-TNF therapy responders and non-responders. **G)** Correlation dot plot comparing $PKN2^{KO}$ score with selected gene set enrichment by GSVA. **H)** Top 50 ranked KEGG gene sets predicting PKN2 function

identified by PrismEXP across the ARCHS4 compendium. **I-K)** Immunohistochemical analysis of distal luminal epithelial ZO-1 staining in mice 8 days following 1% DSS treatment in global-iPKN2^{KO} (I, J; WT: n=4, HET: n=6, KO: n=4) and epithelial-iPKN2^{KO} mice (K; WT: n=4, HET: n=6, KO: n=4; Holm-Šídák's test). Pixel threshold DAB staining intensity shown bottom.

PKN2 loss sensitises intestinal epithelial tight junctions to inflammatory damage

Loss of junctional ZO-1 staining in vivo led us to investigate if PKN2 has a direct role in maintaining junction stability. PKN2 has previously been shown to associate with and regulate apical junction maturation in bronchial epithelial cells[47]. More recently, a study in MDCK-II cells also localised PKN2 to apical junctions as part of the Crumbs complex[48]. Staining of organoids confirms PKN2 is localised to ZO-1 positive apical tight junctions in primary colonic epithelial cells (Figure 4A). Knockout of PKN2 in vitro also reduced ZO-1-positive junction formation in intact organoid cultures (Figure 4B, C). Both junctional ZO-1 staining intensity and junctional area were further reduced in organoids without PKN2 following treatment with 10µg/ml DSS (Figure 4D). While DSS treatment also reduced wild-type organoid junctional area and intensity, no difference was detected in response to 4-hydroxytamoxifen (TAM, Figure S5A-C).

We also explored a tight junction role for PKN2 in colorectal cancer cells as an alternative colonic epithelial model. PKN2 was also localised with ZO-1 in DLD1 and Caco2 colorectal cancer epithelial cell lines (Figure S5D, E). Knockdown of PKN2 using siRNA, or knockout with CRISPR-Cas9, disrupted ZO-1-positive tight junction formation in DLD1 cells (Figure 4E-G, S5F-J). Knockout of PKN2 had minimal effects on adherens junctions in DLD1 cells (Figure S5K). Using the Flp-In T-Rex inducible cell line system (Invitrogen), we produced stable DLD1 cell lines that overexpress wild-type (iDLD1 WT-PKN2) or kinase-dead PKN2 (iDLD1 KD-PKN2 D782A) following tetracycline. Overexpression of KD-PKN2 in iDLD1 cells has a dominant negative effect on junction formation, demonstrating that PKN2 kinase activity is essential for the function of PKN2 in tight junction formation (Figure 4H, I, S6A, B). Overexpression of WT-PKN2 in iDLD1 cells had minimal effects on ZO-1-positive tight junction formation (Figure S6C-F). Analysis of previously published phospho-proteomics data indicates that perturbing PKN2 induces changes in the phosphorylation state of many junctional proteins, including ZO-1 and PARD3, suggesting that PKN2 has a complex role in tight junction formation (Figure S6G)[41, 43].

Tight junctions in colonic epithelia are essential for preventing the influx of luminal pathogens and toxins into the mucosa[49]. The inflammatory phenotypes observed in PKN2-deficient mice are consistent with a sensitisation of epithelial tight junctions that breakdown following DSS induced injury. Functional Transwell™ assays demonstrate PKN2 knockout increases DLD1 epithelial monolayer barrier permeability to fluorescent 40kda FITC-dextran with minimal effects on cell viability (Figure 4J; S5JS6H). In 3D organoid models, loss of PKN2 resulted in an increase in permeability to fluorescent 4kda dextran, but only upon the administration of DSS or inflammatory cocktail (Figure 4K, L). These results demonstrate that epithelial PKN2 is not critical for functional junction homeostasis, but PKN2 loss sensitises tight junctions to inflammatory insult, mirroring our in vivo observations.

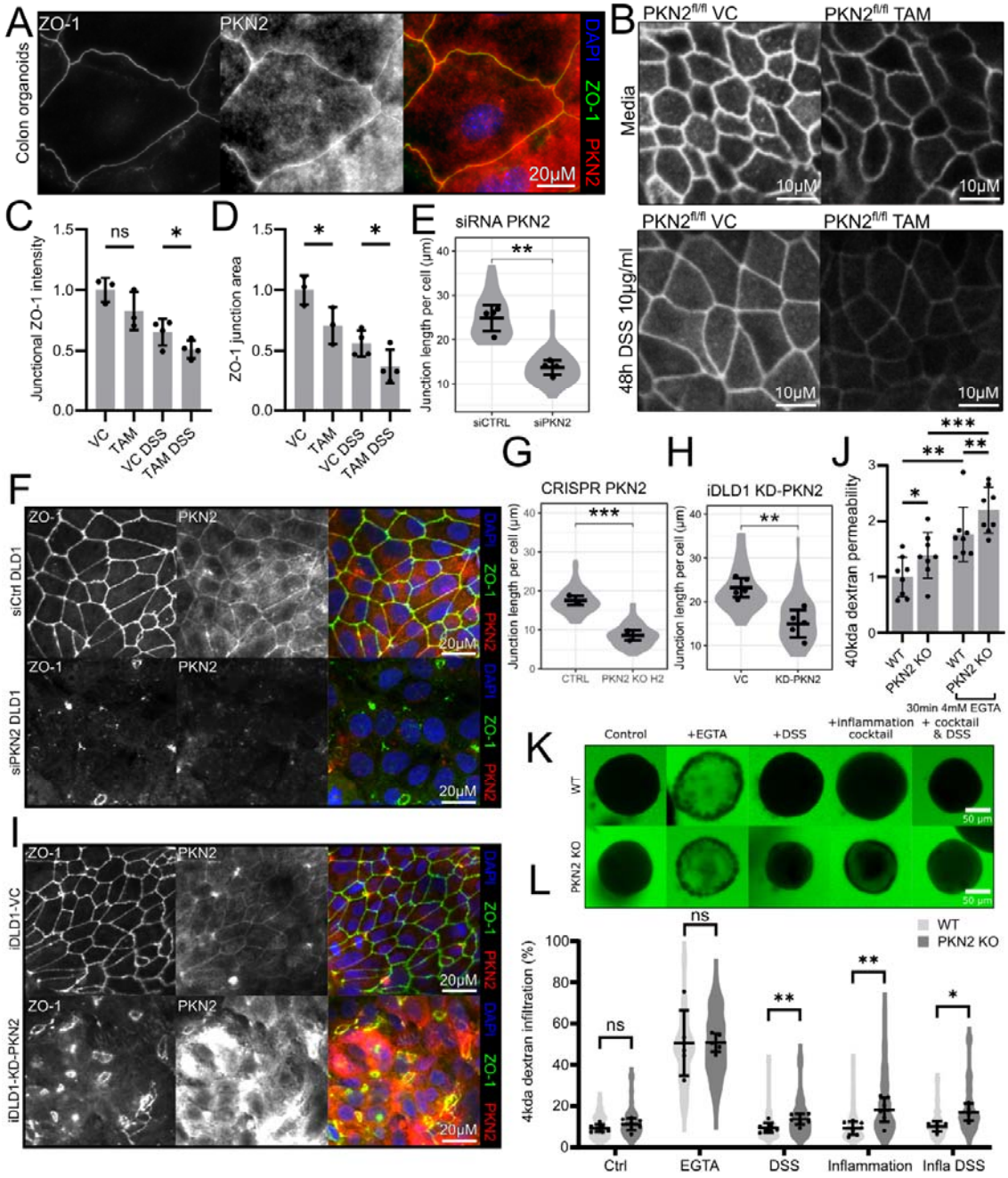

Figure 4: PKN2 loss sensitises intestinal epithelial tight junctions to DSS treatment. A) Immunostaining PKN2 and ZO-1 in C57BL6 colonic organoids cultured in 2D. **B-D)** Quantification of ZO-1 staining intensity and area in primary Rosa$^{Cre/+}$/PKN2$^{fl/fl}$ organoids grown in 3D following 48h treatment with vehicle or 10µg/ml DSS (n=3; Holm-Šídák's test). **E-I)** Disruption of ZO-1 positive tight junction formation following PKN2 depletion by siRNA (E, F), CRISPR (G) or overexpression of a kinase-dead PKN2 (H, I). Tight junction integrity was quantified as average length of junctional ZO-1 per cell (n=4, unpaired, two tailed t-test) **J)** Permeability of CRISPR PKN2^{KO} DLD1 monolayers to 40kda FITC-dextran on 0.4µM Transwells treated with vehicle or 30mins 4mM EGTA (n=8; Fisher's LSD test).

K, L) Permeability of 3D PKN2^{KO} organoids to 4kda FITC-dextran following treatment with 48h 10µg/ml DSS and/or 96h inflammatory cocktail (LPS, IL-1β, IL-6 and TNF-α)(n=7; Tukey's test).

Discussion

Our work identifies *PKN2* as a critical regulator of tight junction formation in the colon, protecting the bowel against inflammatory damage and colorectal cancer initiation. *PKN2*-targeted mice and primary organoids largely maintain morphologically intact tight junctions under homeostatic conditions, but significant defects emerge following epithelial injury, suggesting functional redundancy for normal tissue homeostasis. This concurs with knockout models of other core tight junction components, including O*CLN*, *JAM-A*, *PRKCI*, and *ZO-1*, which maintain homeostatic junctions at baseline but exhibit heightened sensitivity to inflammation and colitis[45, 50-54]. These findings support the notion that homeostatic tight junctions are remarkably resilient to the loss of individual components, yet each contributes critically to maintaining or re-establishing barrier integrity following stress or injury.

Intriguingly, the H.pylori bacteriotoxin CagA, which is known to localise to and disrupt junction formation and cell polarity[55, 56], directly binds to and inhibits the kinase activity of PKN2[57, 58]. Our research suggests that inhibition of PKN2 by CagA, may directly contribute to H.pylori pathogenesis and promotion of colorectal and gastric cancer. Previous research also identified that PKN1 and PKN2 negatively regulate pyrin inflammasome activation in epithelial cells, and their combined knockdown leads to spontaneous IL-1β release, a cytokine known to increase epithelial permeability in colorectal cancer cell lines[59, 60]. However, despite the pro-inflammatory role of IL-1β, multiple knockout models lacking inflammasome components show worsened colitis and AOM-DSS induced tumour burden[61-64]. Furthermore, knockout of PKN2 alone in organoid cultures did not significantly alter IL1B expression, confirming that the tumour-suppressive effects of PKN2 are not primarily mediated through inflammasome dysregulation but instead through direct effects on tight junctions.

PKN2 was identified as one of 25 high-confidence candidate genes within CCs3, a locus associated with the heightened sensitivity of A/J mouse strain to AOM/DSS tumorigenesis, compared to C57BL/6J[17]. Further, PKN2 is among 340 genes within the *Cdcs1* locus, which contributes to enhanced susceptibility to disease in multiple genetic colitis models[16, 65-67]. Here we provide definitive proof that loss of PKN2 alone is sufficient to confer sensitivity to both colitis and colitis-associated-colorectal cancer, establishing PKN2 as a key candidate gene on human chromosome 1p for susceptibility to IBD and colitis-associated-colorectal cancer. PKN2 has also been associated with increased risk of developing irritable bowel syndrome (IBS) in a genome-wide association study (rs10923043)[68] and is one of 16 loci for human periodontitis (rs12032672) and one of 98 loci for rosacea (rs191805855); conditions similarly linked to tight junction integrity and susceptibility to bacterial infiltration in the gums and skin respectively[69-71].

Primary organoids from patients with IBD had a remarkable similarity in their expression profile to primary murine PKN2^{KO} organoids, and PKN2 was identified as one of 18 significantly downregulated genes in endoscopic biopsies from patients with IBD when compared to healthy controls, alongside other junctional components such as PRKCI and CLDN8[72]. This suggests deregulation to core junction components, including PKN2, is a key mechanism of human IBD pathogenesis. In addition, PKN2 lies within 207 genes on the Scc7 locus, which confers susceptibility to DMH-induced sporadic colorectal cancer in the recombinant congenic strain CcS-3 compared with the more resistant BALB/c background[73]. This suggests PKN2 is also a candidate risk factor on human 1p in sporadic colorectal cancer, consistent with the poor prognosis observed in patients with 1p allelic loss.

Author Contributions

J.C.H. and A.J.M.C. conceptualised and developed the study. J.C.H performed the majority of methodology and formal analysis. A.C. contributed cell based and organoid studies. J.C.H. and P.H. conducted RNA sequencing, tissue staining and analysis with help from A.P., K.S. and M.L. J.C.H, J.S., S.M. and A.J.M.C. contributed to in vivo experiments. I.R., I.Q. and A.J.M.C. conducted mouse model development. M.J. and S.M. assisted with pathology and analysis. T.G., N.Q.M. and S.M. supported project development and data collection. J.C.H. and A.J.M.C wrote the manuscript with comments and approval from all the authors.

Competing interests

The authors have no conflicts of interest.

Supplementary

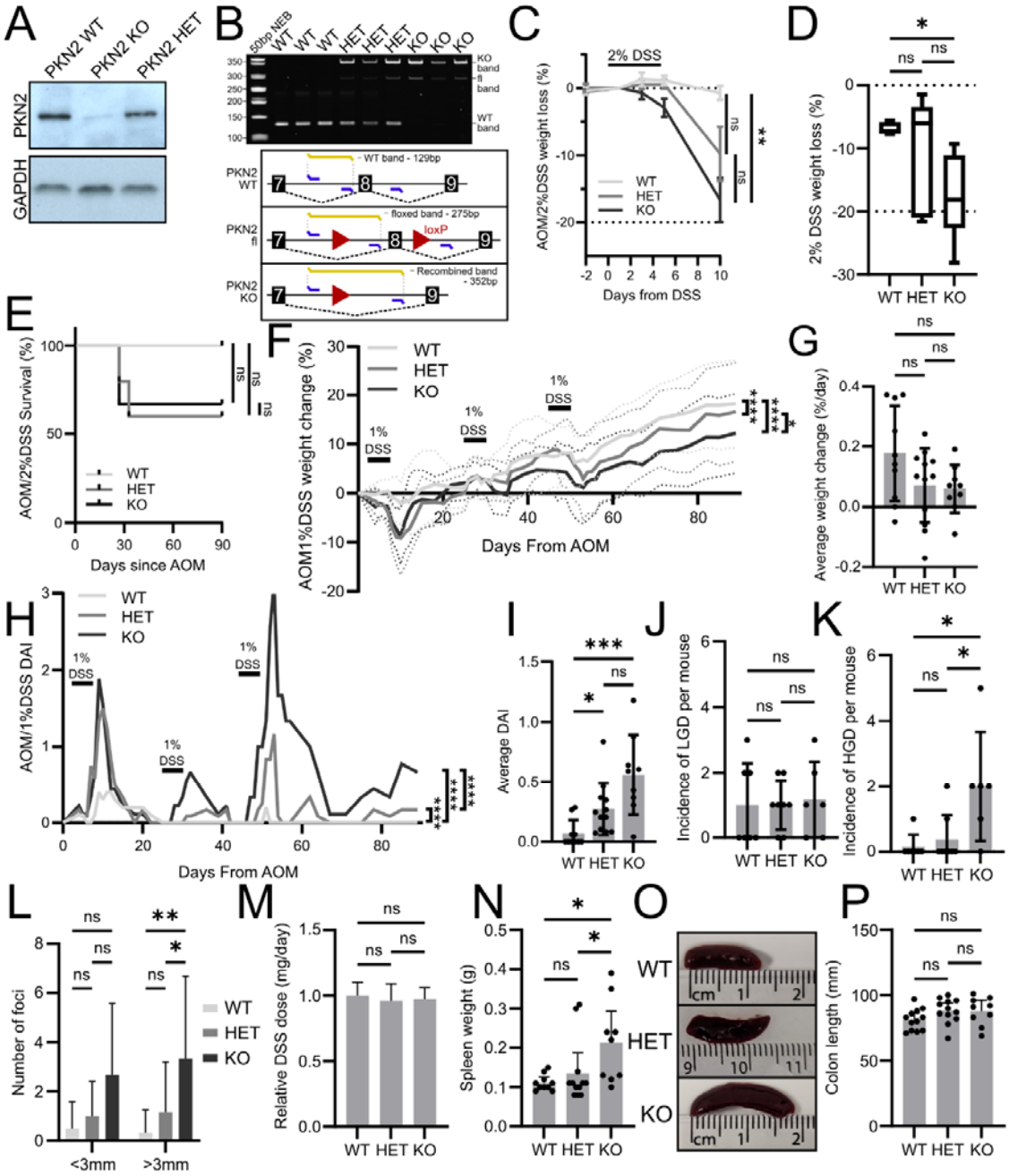

Figure S1: PKN2 loss sensitises mice to DSS treatment. A) PKN2 protein expression of intestinal tissue determined by western blot following the tamoxifen treatment regime. **B)** PCR genotyping of intestinal tissue two weeks following the tamoxifen treatment regime of global-iPKN2^{KO} mice. Schematic describing the primer strategy and expected band sizes is shown in the bottom panel. **C, D)** Average (C) and maximum (D) weight loss in response to the first 10 days of AOM/2%DSS treatment in WT, HET and PKN2 KO mice (WT: n=5, HET: n=5, KO: n=6). Statistical significance was determined using a two-way repeated measures ANOVA (C) or a Dunn's multiple comparisons test (D). E**)** Survival of WT, HET and PKN2 KO mice in response to 1 dose of 10mg/kg AOM followed by 5 days treatment with 100mg/kg tamoxifen and 1 round of 2%DSS for five days (WT: n=17, HET: n=18,

KO: n=17). Statistical significance was determined using a Log-rank test. **F-I)** Average weight loss (F, G) and disease activity scores (H, I) across the second and third rounds of 1%DSS treatment in WT, HET and PKN2 KO mice (WT: n=10, HET: n=12, KO: n=9). Statistical significance was determined using a two-way repeated measures ANOVA (F, H) or a Dunn's multiple comparisons test (G, I). **J, K)** Quantification of low (LGD, J) and high-grade dysplasia (HGD, K) in WT, HET and KO adenomas formed from the AOM/1%DSS treatment protocol (WT: n=7, HET: n=8, KO: n=6). **L)** The average number of small (<3mm) and large (>3mm) diameter macroscopically visible adenomas from the AOM/1%DSS protocol across WT, HET and PKN2 KO mice (WT: n=10, HET: n=12, KO: n=9). **M)** Relative average DSS dose measured through water bottle weight across WT, HET and PKN2 KO mice (WT: n=10, HET: n=12, KO: n=9). **N-P)** Representative image of spleen size (O) and average weight (N) and average colon length (P) in WT, HET and PKN2 KO mice following the full the AOM/1%DSS protocol (WT: n=10, HET: n=12, KO: n=9). Statistical significance was determined using a Tukey's multiple comparisons test.

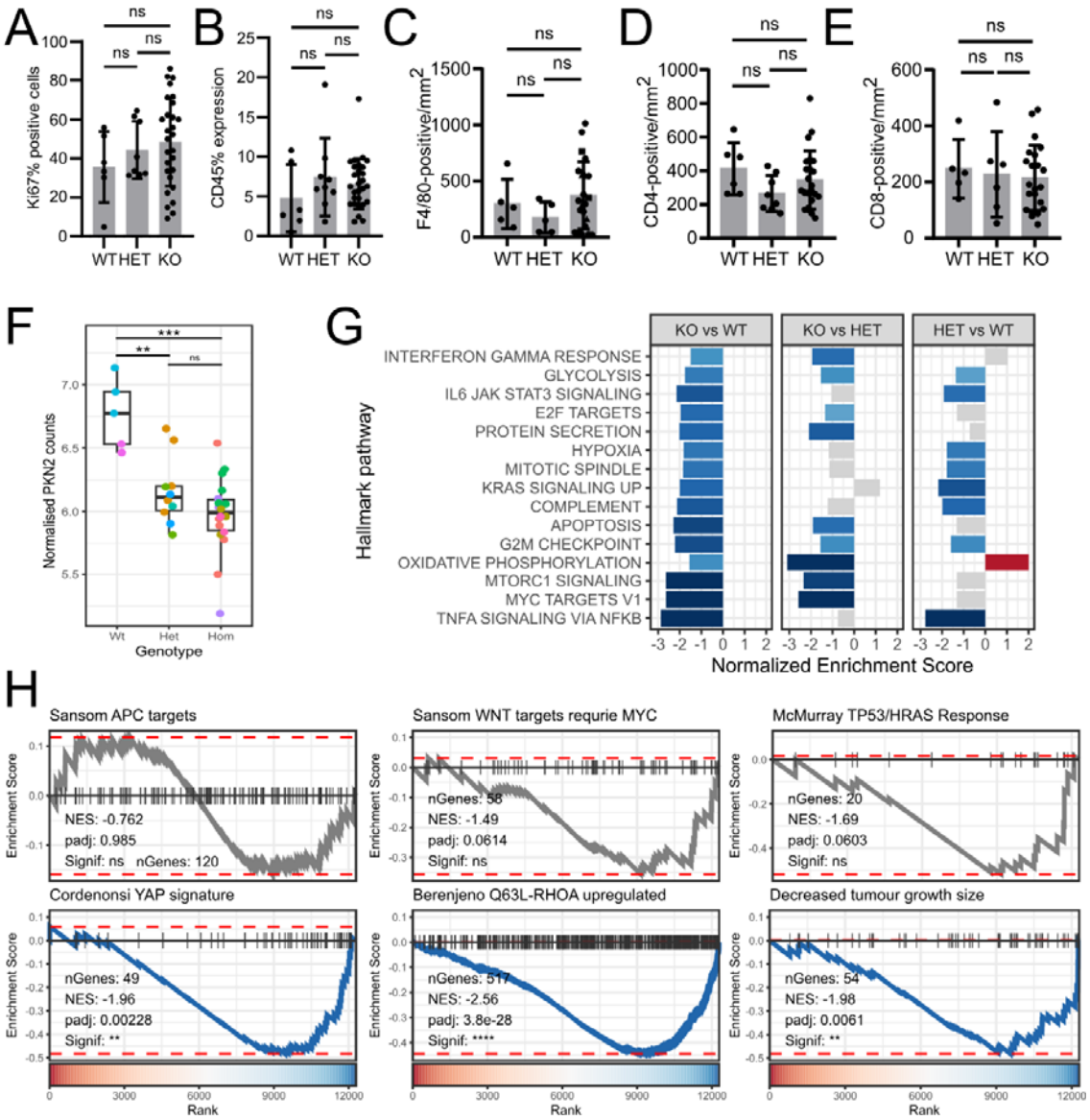

Figure S2: PKN2 status does not dictate tumour phenotype. A-E) Immunohistochemistry analysis of CD45 (A), F4/80 (B), CD4 (C) and CD8 (D) staining in WT, HET and PKN2 KO adenomas formed during the AOM/1%DSS protocol. **F)** PKN2 expression from RNA sequencing analysis in adenomas by genotype. Statistical significance was determined using DESeq2 differential expression analysis (WT: n=5, HET: n=10, KO: n=18). Adenomas from the same individuals are coloured with the same colours. **G)** Gene set enrichment analysis of KO vs WT, KO vs HET and HET vs WT adenomas for the most significant Hallmark gene sets. The top 15 most significant gene sets across all comparisons are shown. **H)** Gene set enrichment analysis of KO vs WT for colorectal Sansom APC and WNT, McMurray TP53/HRAS, Cordenonsi YAP, Berenjeno Q63L-RhoA and mouse phenotypes decreased tumour growth size gene sets.

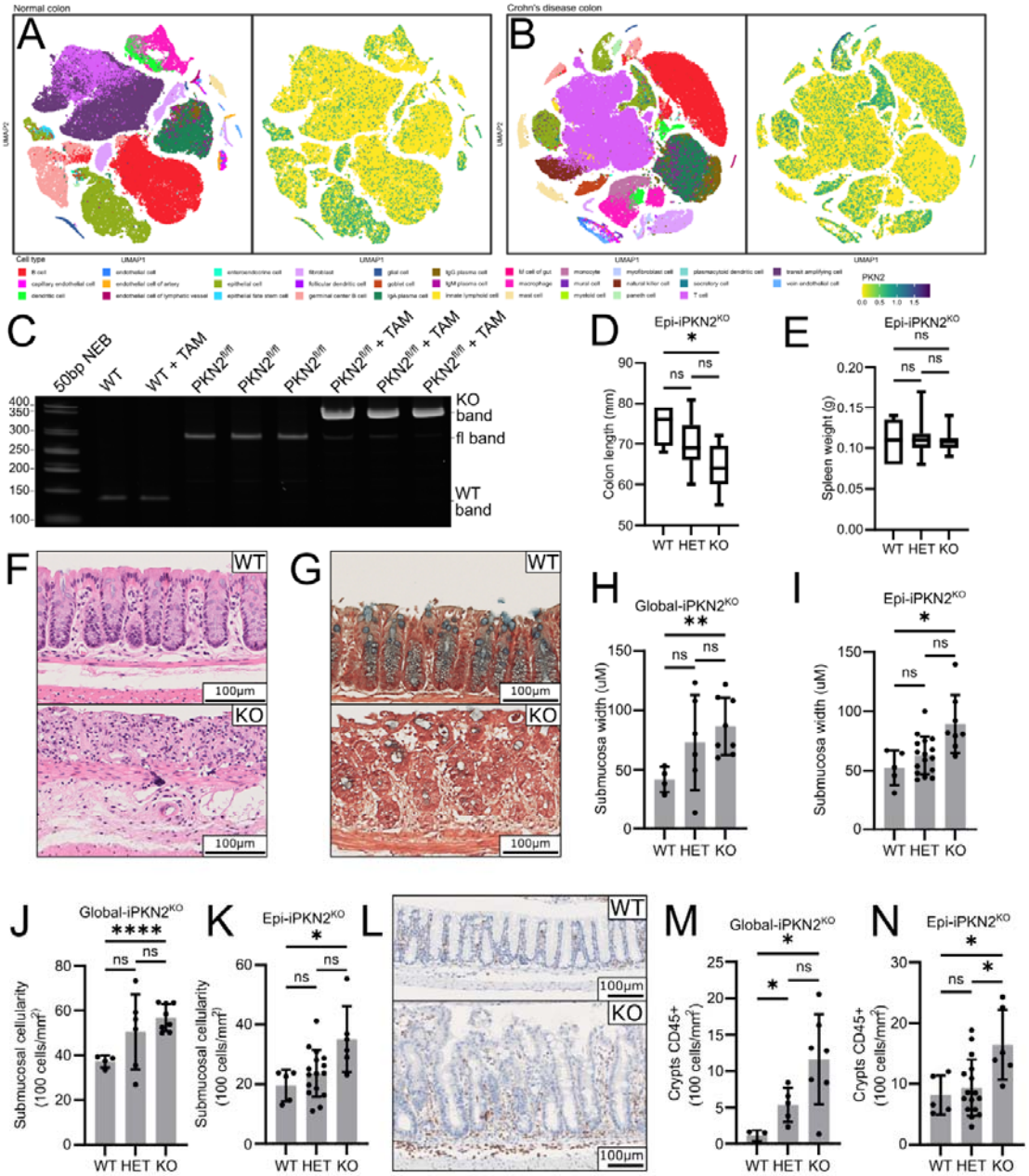

Figure S3: Epithelial specific PKN2 loss induces inflammatory damage. A, B) Single cell RNA sequencing analysis of samples from normal colon (A), Crohn's disease patients (B). Cell subtypes are coloured in the left panel with PKN2 expression labelled in the right panel. **C)** PCR genotyping of isolated colonic epithelial tissue two weeks following the tamoxifen treatment regime in Epi-iPKN2^{KO} mice. Diagram explaining band sizing is in Figure S1C. **D, E)** Colon length (D) and spleen weight (E) in Epi-iPKN2^{KO} mice following 5-days treatment with 2%DSS. Statistical significance was determined using a Dunnett's multiple comparisons test (WT: n=5, HET: n=16, KO: n=8). **F, G)** Epithelial erosion (F) and goblet cell depletion (G) indicated by alcian blue staining in Epi-iPKN2^{KO} mice following 5-days treatment with 2%DSS. **H-K)** Average distal submucosa width (H, I) and cellularity (J, K) in global-iPKN2KO (H, J) and Epi-PKN2KO (I, K) mice following treatment with AOM/1%DSS (H, J) or 2%DSS (I, K). Statistical significance was determined using a Dunnett's multiple comparisons test (H, J: WT: n= 4, HET: n=6, KO: n=8), (I, K: WT: n=5, HET: n=16, KO: n=8). **L-N)** CD45+ immune cell infiltration in distal crypts and submucosa global-iPKN2KO (N) and Epi-PKN2KO (L, N) mice following treatment with AOM/1%DSS (M) or 2%DSS (L, N). Statistical significance was determined using a Dunnett's multiple comparisons test (M: WT: n=3, HET: n=5, KO: n=7) (N: WT: n=5, HET: n=16, KO: n=6).

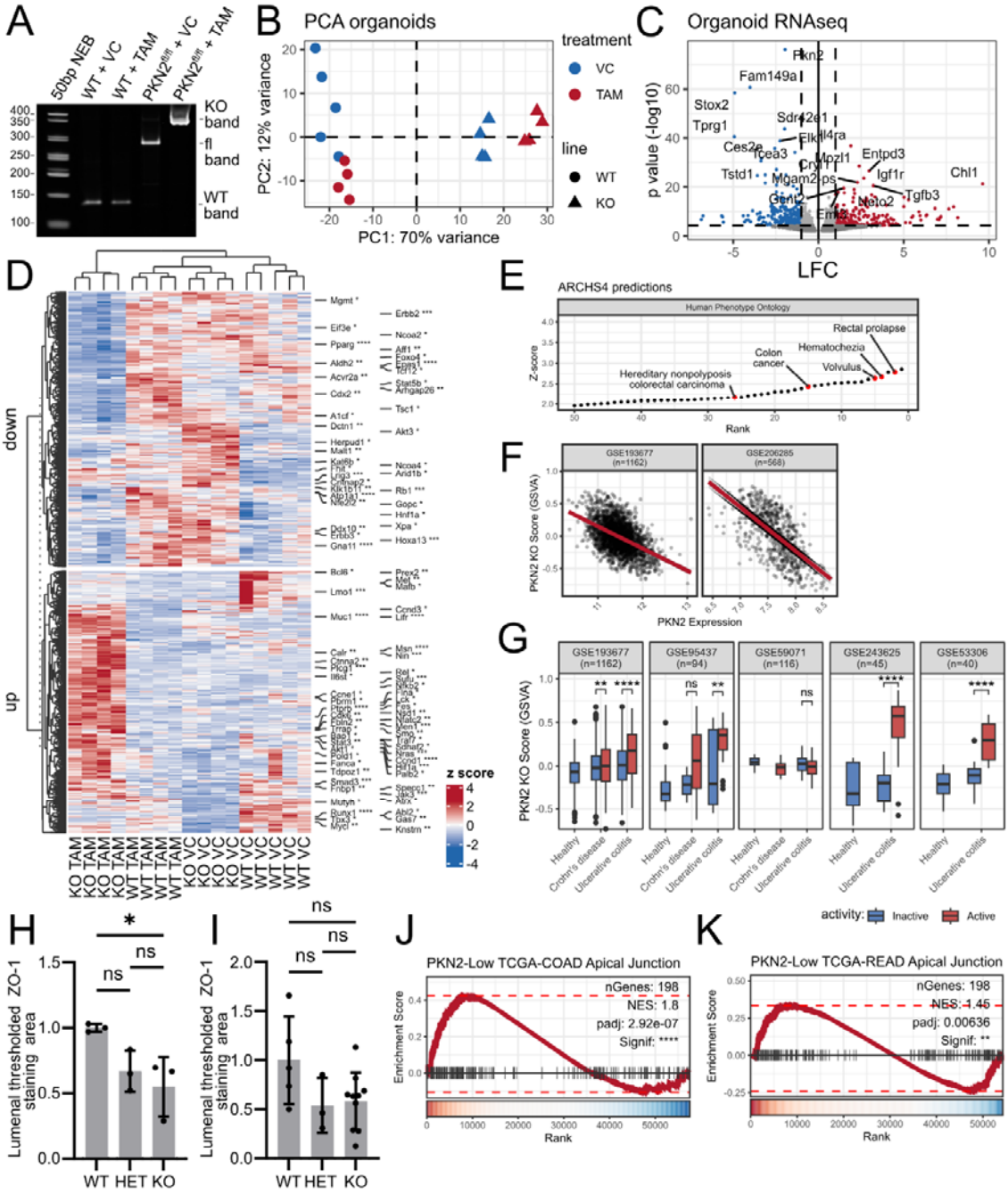

Figure S4: **PKN2 loss alters gene expression, pathway enrichment, and junctional programs in cancer and colitis models. A)** PCR genotyping of colonic organoids one week following the in vitro tamoxifen treatment regime. Diagram explaining band sizing is in Figure S1B. **B)** Principal component analysis of RNA sequencing data from wild-type and Rosa$^{Cre/+}$/PKN2$^{fl/fl}$ primary mouse colon organoids treated with 4-OHT tamoxifen or a vehicle control. **C)** Differential gene expression analysis identifying the most significantly differentially expressed genes between vehicle control and tamoxifen treated PKN2-KO organoids, accounting for the effects of tamoxifen treatment on wild-type organoids. **D)** Significant differentially expressed genes between vehicle control and tamoxifen treated PKN2-KO organoids, accounting for the effects of tamoxifen treatment on wild-type

organoids. Known cancer genes from the Cancer Gene Consensus are labelled. **E)** Top 50 ranked human phenotype ontology gene sets for predictions of PKN2 function by PrismEXP across the ARCHS4 compendium. **F)** Scatter plots describing the relationship between PKN2 expression and PKN2 knockout score. **G)** Differences in PKN2 KO score comparing patients with active and inactive disease. **H, I)** Immunohistochemical analysis of distal colonic luminal epithelial ZO-1 staining in mice two weeks following PKN2 knockout induction (H) or 15 days following the initiation of 5 days of 1% DSS treatment (I). Statistical significance was determined using a Holm-Šídák's multiple comparisons test (H: n=9, I: n=18). **J, K)** GSEA of hallmark apical junction gene set in TCGA-COAD (J) and TCGA-READ (K) ranks created from comparing PKN2-low and PKN2-high patient primary tumours.

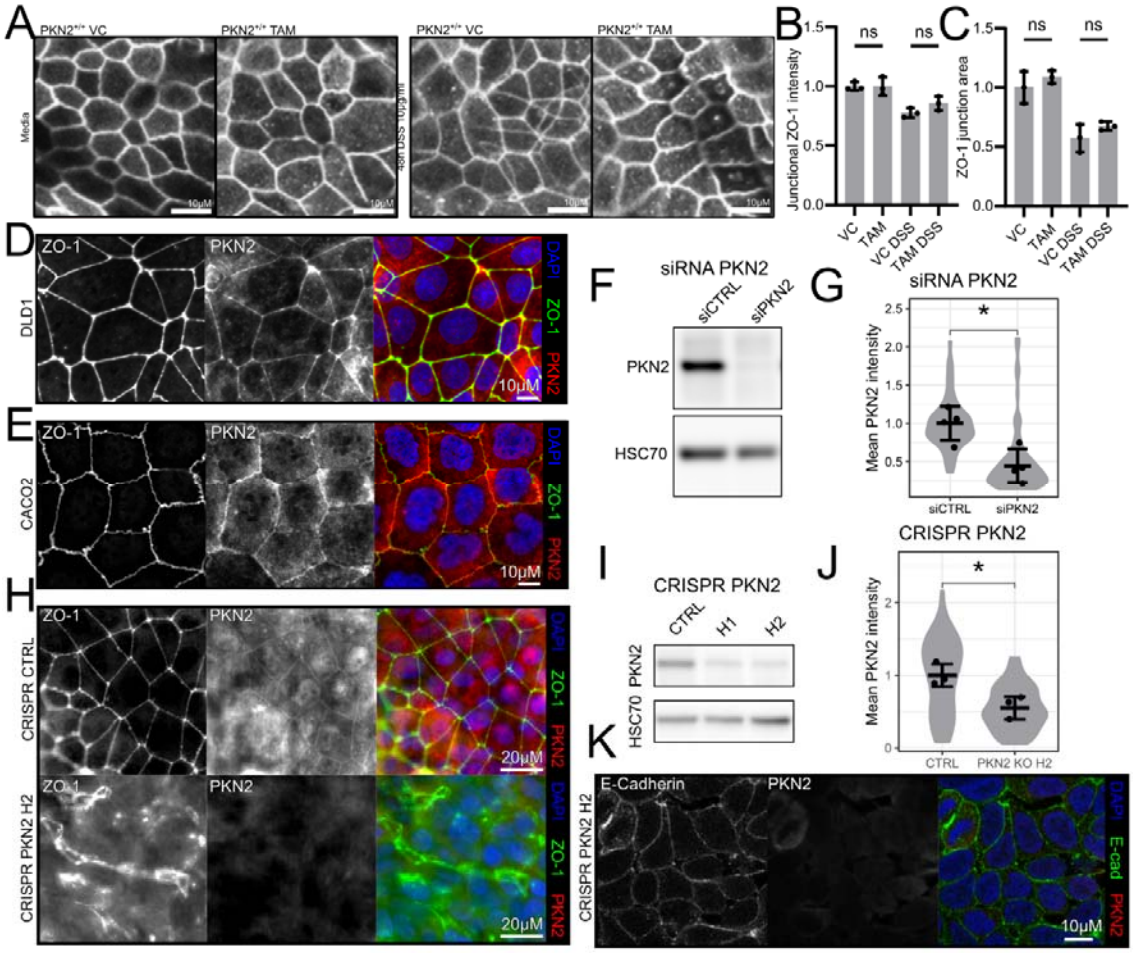

Figure S5: PKN2 regulates junctional ZO-1 integrity in cells, organoids, and mouse colon epithelium. A-C) Staining of ZO-1 in primary wild-type mouse organoids following 48h treatment with vehicle control or 48h 10µg/ml DSS. Graphs demonstrate a loss of junctional ZO-1 staining area (F) and intensity (G) following DSS treatment but no difference upon application of 4-OHT (TAM). Statistical significance was determined using a Holm-Šídák's multiple comparisons test (n=3). **D, E)** Colocalization staining of junctional PKN2 and ZO-1 in DLD1 (A) and CACO2 (B) cells. **F-J)** Loss of PKN2 protein expression (F, G, I, J) and loss of ZO-1 positive tight junction formation (H) following PKN2 knockdown with a PKN2-targeting siRNA pool (F, G) or PKN2 knockout using CRISPR (H-J) by immunofluorescence and western blot analysis. Statistical significance was determined using an

unpaired, two-tailed t-test (n=4). **K)** E-cadherin staining of adherens junctions in CRISPR PKN2 knockout DLD1 cells.

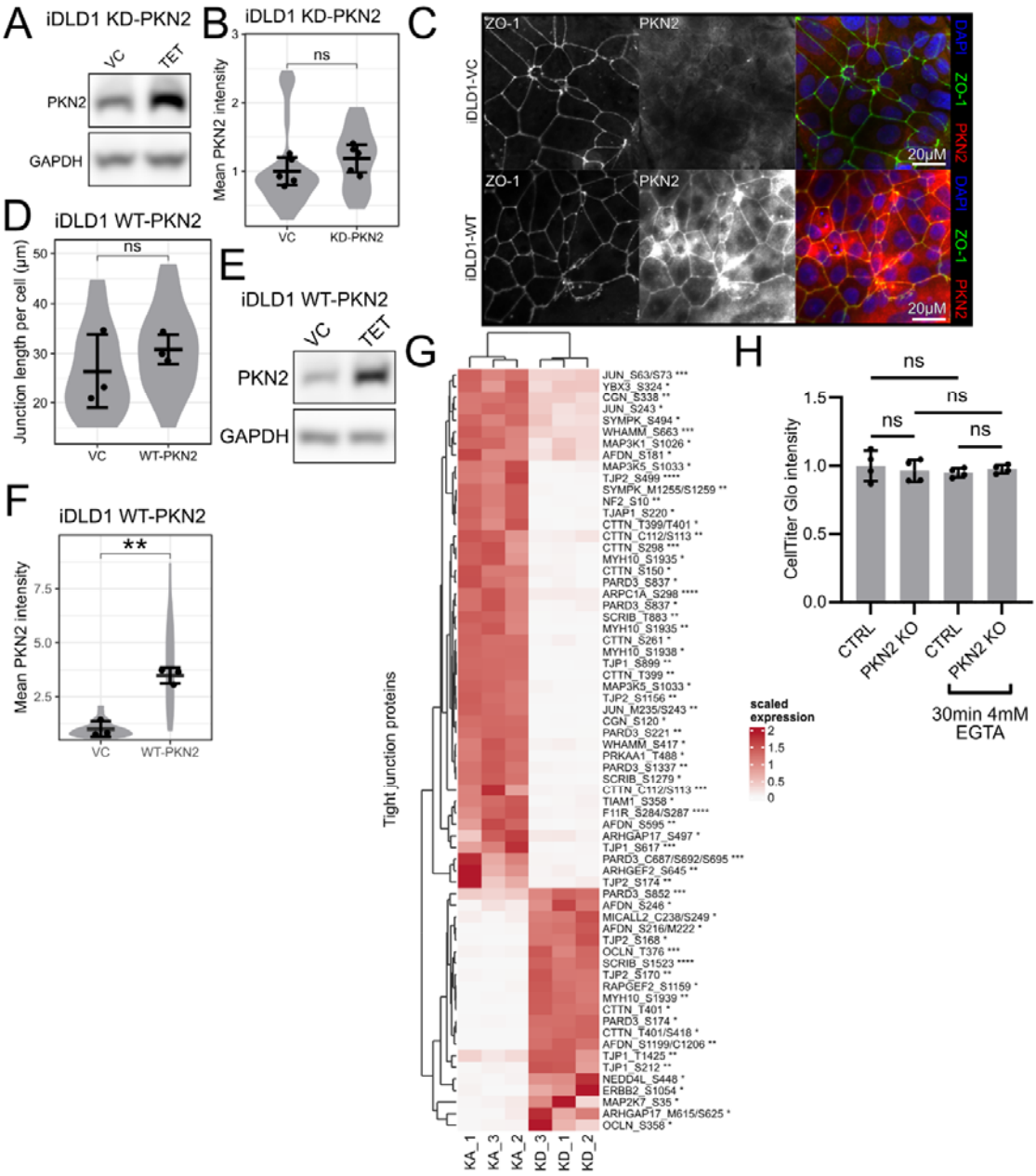

Figure S6: Impact of PKN2 knockout and overexpression on adherens and tight junctions. A, B) Gain of PKN2 expression following overexpression of a kinase-dead (KD) PKN2 in the inducible DLD1 cell line (iDLD1) (n=5; unpaired, two-tailed t-test). **C-F)** Change in average junction length per cell (C, D) and gain in PKN2 expression (C, E, F) following overexpression of wild-type PKN2 (n=3; unpaired, two-tailed t-test). **G)** Heatmap of significant changes to the phosphoproteome of junction proteins with overexpression of kinase dead versus kinase active PKN2. **H)** Difference in in CellTitre Glo intensity between CRISPR control and PKN2 KO gRNA DLD1 lines.

Acknowledgements

We thank the core services at the Barts Cancer Institute, including Biological Services, Animal Technician Services, Pathology, Preclinical Imaging, and Microscopy. We are also grateful to Queen Mary's Apocrita HPC facility, supported by QMUL Research-IT, and to the Phenotypic Screening Facility at the Blizzard Institute. We acknowledge the Genomics Facility at the Institute of Cancer Research. We also thank Professor Peter Parker and Ian Rosewell for their help in developing the PKN2-targeted mice. Finally, we are grateful to the laboratories of Shinta Sato, and Egle Solito for supplying L-WRN and Caco2 cells.

References

1. Ng SC, Shi HY, Hamidi N, et al. Worldwide incidence and prevalence of inflammatory bowel disease in the 21st century: a systematic review of population-based studies. Lancet 2017;390:2769-2778.
2. Ekbom A, Helmick C, Zack M, et al. Ulcerative colitis and colorectal cancer. A population-based study. N Engl J Med 1990;323:1228-33.
3. Eaden JA, Abrams KR, Mayberry JF. The risk of colorectal cancer in ulcerative colitis: a meta-analysis. Gut 2001;48:526-35.
4. Gyde SN, Prior P, Allan RN, et al. Colorectal cancer in ulcerative colitis: a cohort study of primary referrals from three centres. Gut 1988;29:206-17.
5. Baron JA, Cole BF, Sandler RS, et al. A randomized trial of aspirin to prevent colorectal adenomas. N Engl J Med 2003;348:891-9.
6. Cole BF, Logan RF, Halabi S, et al. Aspirin for the chemoprevention of colorectal adenomas: meta-analysis of the randomized trials. J Natl Cancer Inst 2009;101:256-66.
7. Bertagnolli MM, Eagle CJ, Zauber AG, et al. Celecoxib for the prevention of sporadic colorectal adenomas. N Engl J Med 2006;355:873-84.
8. Baron JA, Sandler RS, Bresalier RS, et al. A randomized trial of rofecoxib for the chemoprevention of colorectal adenomas. Gastroenterology 2006;131:1674-82.
9. Jamieson T, Clarke M, Steele CW, et al. Inhibition of CXCR2 profoundly suppresses inflammation-driven and spontaneous tumorigenesis. J Clin Invest 2012;122:3127-44.
10. Grivennikov S, Karin E, Terzic J, et al. IL-6 and Stat3 are required for survival of intestinal epithelial cells and development of colitis-associated cancer. Cancer Cell 2009;15:103-13.
11. Putoczki TL, Thiem S, Loving A, et al. Interleukin-11 is the dominant IL-6 family cytokine during gastrointestinal tumorigenesis and can be targeted therapeutically. Cancer Cell 2013;24:257-71.
12. Greten FR, Eckmann L, Greten TF, et al. IKKbeta links inflammation and tumorigenesis in a mouse model of colitis-associated cancer. Cell 2004;118:285-96.
13. Cho JH, Nicolae DL, Gold LH, et al. Identification of novel susceptibility loci for inflammatory bowel disease on chromosomes 1p, 3q, and 4q: evidence for epistasis between 1p and IBD1. Proc Natl Acad Sci U S A 1998;95:7502-7.
14. Cho JH, Nicolae DL, Ramos R, et al. Linkage and linkage disequilibrium in chromosome band 1p36 in American Chaldeans with inflammatory bowel disease. Hum Mol Genet 2000;9:1425-32.
15. El Hadad J, Schreiner P, Vavricka SR, et al. The Genetics of Inflammatory Bowel Disease. Mol Diagn Ther 2024;28:27-35.
16. Ermann J, Garrett WS, Kuchroo J, et al. Severity of innate immune-mediated colitis is controlled by the cytokine deficiency-induced colitis susceptibility-1 (Cdcs1) locus. Proc Natl Acad Sci U S A 2011;108:7137-41.
17. Meunier C, Cai J, Fortin A, et al. Characterization of a major colon cancer susceptibility locus (Ccs3) on mouse chromosome 3. Oncogene 2010;29:647-61.

18. Quetier I, Marshall JJ, Spencer-Dene B, et al. Knockout of the PKN Family of Rho Effector Kinases Reveals a Non-redundant Role for PKN2 in Developmental Mesoderm Expansion. Cell Rep 2016;14:440-8.
19. Cooper HS, Murthy SN, Shah RS, et al. Clinicopathologic study of dextran sulfate sodium experimental murine colitis. Lab Invest 1993;69:238-49.
20. Moolenbeek C, Ruitenberg EJ. The "Swiss roll": a simple technique for histological studies of the rodent intestine. Lab Anim 1981;15:57-9.
21. Bankhead P, Loughrey MB, Fernandez JA, et al. QuPath: Open source software for digital pathology image analysis. Sci Rep 2017;7:16878.
22. Takahashi Y, Sato S, Kurashima Y, et al. A Refined Culture System for Human Induced Pluripotent Stem Cell-Derived Intestinal Epithelial Organoids. Stem Cell Reports 2018;10:314-328.
23. Qin X, Sufi J, Vlckova P, et al. Cell-type-specific signaling networks in heterocellular organoids. Nat Methods 2020;17:335-342.
24. Giuliano CJ, Lin A, Girish V, et al. Generating Single Cell-Derived Knockout Clones in Mammalian Cells with CRISPR/Cas9. Curr Protoc Mol Biol 2019;128:e100.
25. Foley JW, Zhu C, Jolivet P, et al. Gene expression profiling of single cells from archival tissue with laser-capture microdissection and Smart-3SEQ. Genome Res 2019;29:1816-1825.
26. Passman AM, Haughey MJ, Carlotti E, et al. Hepatocytes undergo punctuated expansion dynamics from a periportal stem cell niche in normal human liver. J Hepatol 2023;79:417-432.
27. Sarvestani SK, Signs SA, Lefebvre V, et al. Cancer-predicting transcriptomic and epigenetic signatures revealed for ulcerative colitis in patient-derived epithelial organoids. Oncotarget 2018;9:28717-28730.
28. Argmann C, Hou R, Ungaro RC, et al. Biopsy and blood-based molecular biomarker of inflammation in IBD. Gut 2023;72:1271-1287.
29. Pavlidis P, Tsakmaki A, Pantazi E, et al. Interleukin-22 regulates neutrophil recruitment in ulcerative colitis and is associated with resistance to ustekinumab therapy. Nat Commun 2022;13:5820.
30. Haberman Y, Karns R, Dexheimer PJ, et al. Ulcerative colitis mucosal transcriptomes reveal mitochondriopathy and personalized mechanisms underlying disease severity and treatment response. Nat Commun 2019;10:38.
31. Pavlidis P, Tsakmaki A, Treveil A, et al. Cytokine responsive networks in human colonic epithelial organoids unveil a molecular classification of inflammatory bowel disease. Cell Rep 2022;40:111439.
32. Arijs I, De Hertogh G, Lemaire K, et al. Mucosal gene expression of antimicrobial peptides in inflammatory bowel disease before and after first infliximab treatment. PLoS One 2009;4:e7984.
33. Vanhove W, Peeters PM, Staelens D, et al. Strong Upregulation of AIM2 and IFI16 Inflammasomes in the Mucosa of Patients with Active Inflammatory Bowel Disease. Inflamm Bowel Dis 2015;21:2673-82.
34. Boyd M, Thodberg M, Vitezic M, et al. Characterization of the enhancer and promoter landscape of inflammatory bowel disease from human colon biopsies. Nat Commun 2018;9:1661.
35. Garrido-Trigo A, Corraliza AM, Veny M, et al. Macrophage and neutrophil heterogeneity at single-cell spatial resolution in human inflammatory bowel disease. Nat Commun 2023;14:4506.
36. Song EM, Saqib J, Joo YH, et al. Inflammatory transcriptomic signatures and cell type compositions in inflamed and non-inflamed colonic mucosa of ulcerative colitis. Genes Dis 2025;12:101447.

37. Zhao X, Fan J, Zhi F, et al. Mobilization of epithelial mesenchymal transition genes distinguishes active from inactive lesional tissue in patients with ulcerative colitis. Hum Mol Genet 2015;24:4615-24.
38. Leal RF, Planell N, Kajekar R, et al. Identification of inflammatory mediators in patients with Crohn's disease unresponsive to anti-TNFalpha therapy. Gut 2015;64:233-42.
39. Avram V, Yadav S, Sahasrabudhe P, et al. IBDTransDB: a manually curated transcriptomic database for inflammatory bowel disease. Database (Oxford) 2024;2024.
40. Haberman Y, Tickle TL, Dexheimer PJ, et al. Pediatric Crohn disease patients exhibit specific ileal transcriptome and microbiome signature. J Clin Invest 2014;124:3617-33.
41. Killarney ST, Mesa G, Washart R, et al. PKN2 Is a Dependency of the Mesenchymal-like Cancer Cell State. Cancer Discov 2025;15:595-615.
42. Lachmann A, Rizzo KA, Bartal A, et al. PrismEXP: gene annotation prediction from stratified gene-gene co-expression matrices. PeerJ 2023;11:e14927.
43. Murray ER, Menezes S, Henry JC, et al. Disruption of pancreatic stellate cell myofibroblast phenotype promotes pancreatic tumor invasion. Cell Rep 2022;38:110227.
44. De Robertis M, Massi E, Poeta ML, et al. The AOM/DSS murine model for the study of colon carcinogenesis: From pathways to diagnosis and therapy studies. J Carcinog 2011;10:9.
45. Kuo WT, Zuo L, Odenwald MA, et al. The Tight Junction Protein ZO-1 Is Dispensable for Barrier Function but Critical for Effective Mucosal Repair. Gastroenterology 2021;161:1924-1939.
46. Poritz LS, Garver KI, Green C, et al. Loss of the tight junction protein ZO-1 in dextran sulfate sodium induced colitis. J Surg Res 2007;140:12-9.
47. Wallace SW, Magalhaes A, Hall A. The Rho target PRK2 regulates apical junction formation in human bronchial epithelial cells. Mol Cell Biol 2011;31:81-91.
48. Tan B, Yatim S, Peng S, et al. The Mammalian Crumbs Complex Defines a Distinct Polarity Domain Apical of Epithelial Tight Junctions. Curr Biol 2020;30:2791-2804 e6.
49. Paradis T, Begue H, Basmaciyan L, et al. Tight Junctions as a Key for Pathogens Invasion in Intestinal Epithelial Cells. Int J Mol Sci 2021;22.
50. Saitou M, Furuse M, Sasaki H, et al. Complex phenotype of mice lacking occludin, a component of tight junction strands. Mol Biol Cell 2000;11:4131-42.
51. Schulzke JD, Gitter AH, Mankertz J, et al. Epithelial transport and barrier function in occludin-deficient mice. Biochim Biophys Acta 2005;1669:34-42.
52. Khounlotham M, Kim W, Peatman E, et al. Compromised intestinal epithelial barrier induces adaptive immune compensation that protects from colitis. Immunity 2012;37:563-73.
53. Laukoetter MG, Nava P, Lee WY, et al. JAM-A regulates permeability and inflammation in the intestine in vivo. J Exp Med 2007;204:3067-76.
54. Calcagno SR, Li S, Shahid MW, et al. Protein kinase C iota in the intestinal epithelium protects against dextran sodium sulfate-induced colitis. Inflamm Bowel Dis 2011;17:1685-97.
55. Amieva MR, Vogelmann R, Covacci A, et al. Disruption of the epithelial apical-junctional complex by Helicobacter pylori CagA. Science 2003;300:1430-4.
56. Buti L, Ruiz-Puig C, Sangberg D, et al. CagA-ASPP2 complex mediates loss of cell polarity and favors H. pylori colonization of human gastric organoids. Proc Natl Acad Sci U S A 2020;117:2645-2655.
57. Nesic D, Buti L, Lu X, et al. Structure of the Helicobacter pylori CagA oncoprotein bound to the human tumor suppressor ASPP2. Proc Natl Acad Sci U S A 2014;111:1562-7.
58. Mishra JP, Cohen D, Zamperone A, et al. CagA of Helicobacter pylori interacts with and inhibits the serine-threonine kinase PRK2. Cell Microbiol 2015;17:1670-82.
59. Park YH, Wood G, Kastner DL, et al. Pyrin inflammasome activation and RhoA signaling in the autoinflammatory diseases FMF and HIDS. Nat Immunol 2016;17:914-21.

60. Duffy HS, John GR, Lee SC, et al. Reciprocal regulation of the junctional proteins claudin-1 and connexin43 by interleukin-1beta in primary human fetal astrocytes. J Neurosci 2000;20:RC114.
61. Sharma D, Malik A, Guy CS, et al. Pyrin Inflammasome Regulates Tight Junction Integrity to Restrict Colitis and Tumorigenesis. Gastroenterology 2018;154:948-964 e8.
62. Hu B, Elinav E, Huber S, et al. Inflammation-induced tumorigenesis in the colon is regulated by caspase-1 and NLRC4. Proc Natl Acad Sci U S A 2010;107:21635-40.
63. Allen IC, TeKippe EM, Woodford RM, et al. The NLRP3 inflammasome functions as a negative regulator of tumorigenesis during colitis-associated cancer. J Exp Med 2010;207:1045-56.
64. Salcedo R, Worschech A, Cardone M, et al. MyD88-mediated signaling prevents development of adenocarcinomas of the colon: role of interleukin 18. J Exp Med 2010;207:1625-36.
65. Mahler M, Most C, Schmidtke S, et al. Genetics of colitis susceptibility in IL-10-deficient mice: backcross versus F2 results contrasted by principal component analysis. Genomics 2002;80:274-82.
66. Farmer MA, Sundberg JP, Bristol IJ, et al. A major quantitative trait locus on chromosome 3 controls colitis severity in IL-10-deficient mice. Proc Natl Acad Sci U S A 2001;98:13820-5.
67. Borm ME, He J, Kelsall B, et al. A major quantitative trait locus on mouse chromosome 3 is involved in disease susceptibility in different colitis models. Gastroenterology 2005;128:74-85.
68. Bonfiglio F, Zheng T, Garcia-Etxebarria K, et al. Female-Specific Association Between Variants on Chromosome 9 and Self-Reported Diagnosis of Irritable Bowel Syndrome. Gastroenterology 2018;155:168-179.
69. Divaris K, Monda KL, North KE, et al. Genome-wide association study of periodontal pathogen colonization. J Dent Res 2012;91:21S-28S.
70. Chen LX, Hao PS. The role of skin barrier and immune abnormalities in the pathogenesis of Rosacea. Clin Exp Med 2025;25:324.
71. Puzhankara L, Rajagopal A, Kedlaya MN, et al. Cell Junctions in Periodontal Health and Disease: An Insight. Eur J Dent 2024;18:448-457.
72. Wu F, Dassopoulos T, Cope L, et al. Genome-wide gene expression differences in Crohn's disease and ulcerative colitis from endoscopic pinch biopsies: insights into distinctive pathogenesis. Inflamm Bowel Dis 2007;13:807-21.
73. van Wezel T, Ruivenkamp CA, Stassen AP, et al. Four new colon cancer susceptibility loci, Scc6 to Scc9 in the mouse. Cancer Res 1999;59:4216-8.